Review

Structural comparison of contractile nanomachines

Sebastian Kube and Petra Wendler *

Gene Center Munich, Ludwig-Maximilians-Universität München, Feodor-Lynen-Strasse 25, D-81377 Munich, Germany

* Correspondence: Email: wendler@genzentrum.lmu.de; Tel: +49-(0)89-2180-76928.

Abstract: Contractile molecular machines are a common feature among bacteriophages and prokaryotes. Due to their stability and the large size, contractile-tailed bacteriophages are traditionally investigated by electron microscopic methods. Complemented by crystallographic studies, a molecular model of contraction for the T4 phage was developed. Lately, also related contractile structures like the *Photorhabdus* virulence cassette-like particles, the R-Type pyocins and the contractile tubule of the bacterial Type VI secretion system have been analyzed by cryo electron microscopy. *Photorhabdus* virulence cassette particles and R-Type pyocins are toxin complexes reminiscent of bacteriophage tails that are secreted by bacteria to kill their insect host or competing bacteria. In contrast, the Type VI secretion system is an intracellular apparatus for injection of effector proteins into bacterial and eukaryotic cells. Although it shares homology with other contractile systems, the Type VI secretion system is additionally equipped with a recycling function, which makes it suitable for multiple rounds of action. Starting from the 3D reconstructions, we compare these molecular machines structurally and functionally to their viral counterparts and summarize the current knowledge on their respective mode of action.

1. Contractile Phage-tail-like Structures in Viruses and Prokaryotes

Contractile molecular machines have first been identified in bacterial viruses [1], but similar structures have also been found in many prokaryotes, e. g. R-type pyocins [2], the Type VI secretion system (T6SS) and phage tail-like protein translocation structures (PLTS) [3]. They are large multimeric protein complexes, which have been investigated for decades by electron microscopic (EM) three-dimensional reconstruction methods. Initially, 3D EM reconstructions were focused on the T4 bacteriophage tail, first embedded in heavy-metal stain [4], and much later also in vitreous

ice [5,6]. In the recent years reconstructions of other bacteriophage tails [7–10], a pyocin [11], the T6SS contractile machinery [12–15], and PLTS followed [16,17].

As suggested recently by Sarris and colleagues after phylogenetic analysis of structural genes common to all contractile systems, phage tail-like structures can be classified into contractile phage tails, R-type pyocins, PLTS and the T6SS (Figure 1) [3]. Pairwise-similarity clustering of sequences of proteins forming the contractile sheaths alone leads to a comparable classification. T6SS sheath proteins are the most distinct from all others, whereas PLTS sheath proteins are similar to the T4 sheath protein. R-Type pyocin sheath proteins from *Pseudomonas aeruginosa* resemble those of phage P2 while another pyocin from *Clostridum difficile* is more similar to two sheath proteins (Lin1278 and DSY3957), which resemble T4 phage sheath proteins [9]. The T6SS cluster clearly reflects also a functional difference to the other systems, as it acts intracellularly and is not secreted. However, analysis of structural similarities between the building blocks of all systems is highly suggestive of a "single protein module" as a common ancestor which has been first arisen in viruses and which was then acquired by bacteria [18]. In this review, we compare the known phage tail-like systems structurally and functionally, summarizing the current knowledge as an introduction to the field but do not hypothesize on evolutionary coherencies. There are many excellent reviews on the structure of contractile phage tails [1,19], the structural biology of the T6SS [20,21,22], pyocins [2], and evolutionary relationship of these systems [18]. An excellent comparison of all four systems in their composition and functionalities can be found in Sarris et al. (2014) and they are also juxtaposed in table 1 based on [1,3,23]. We refer the interested reader to these publications for an in-depth coverage of these topics. Since bacteriophage T4 has been investigated the most thoroughly, among bacteriophages and among all contractile systems, we will generally use its nomenclature except for the type VI secretion system, as it is the most divergent class.

1.1. Contractile bacteriophages

Tailed bacteriophages form the most common group of bacterial viruses. About 96% of all known bacteriophages belong to this order (Caudovirales). A quarter of them belongs to the family of Myoviridae, which consist of a cubic head holding dsDNA, and a helical contractile tail separated from the head by a short neck [26]. The tail ends in a baseplate structure, which is decorated with tail fibers. For infection, the bacteriophage attaches to characteristic surface structures on the host cell with its fibers. This induces a conformational change in the fibers, which is transmitted to the baseplate to trigger sheath contraction. Upon contraction, the needle complex is ejected, piercing the host cell membrane. Subsequently the viral DNA is released through the hollow needle and transferred to the cytosol [19]. After infection the host cell protein production machinery is captured to produce new viral particles which are then released by cell lysis (lytic infection) [27].

The bacteriophage T4 serves as a model system for all contractile protein machines and has been investigated for over 73 years using electron microscopic methods [28,29]. In fact, the elongated T4 phage tail was the first sample investigated by EM three-dimensional image reconstruction methods [30]. The T4 assembly, architecture and proposed contraction mechanism has been reviewed elsewhere [1,19].
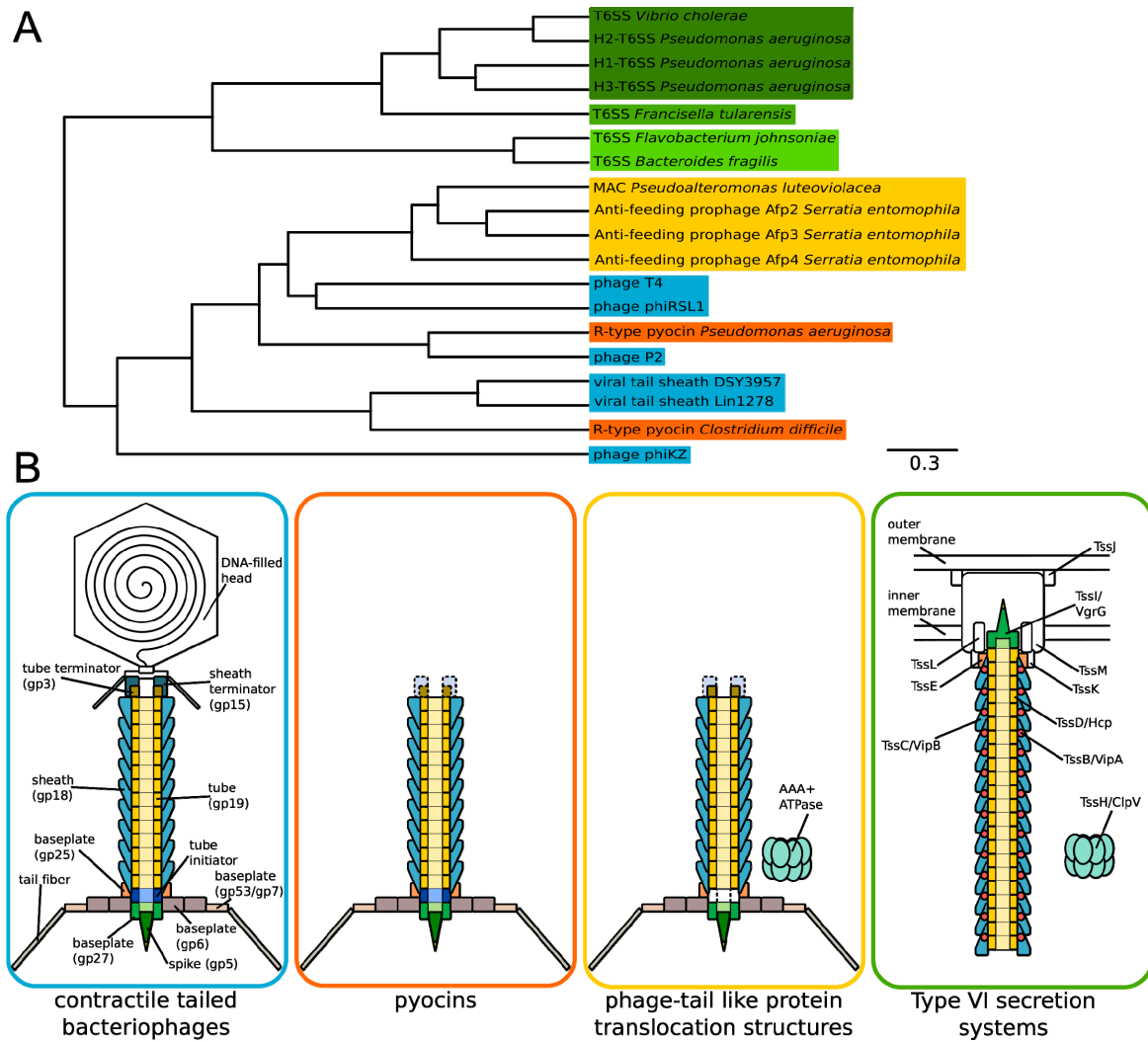
Figure 1. Classification of contractile phage-like structures based on their sheath proteins. (A) Sheath proteins have been aligned using MSAProbs [24] and clustered using the UPGMA method in PHYLIP-NEIGHBOR [25] which reproduces the four families of contractile phage like structures as described [3]: contractile bacteriophages (blue), pyocins (orange), Type VI secretion system (T6SS) families I-III (green) and other phage tail-like protein translocation structures (PLTS, yellow). T6S sheath proteins TssB and TssC are concatenated for the alignment. (B) Schematic overview of known or suspected structural homologs in contractile phage-like assemblies. Similar parts of the contractile machinery are presented in identical color. Unidentified but suspected homologous parts are depicted in broken lines. *From left to right:* contractile tailed bacteriophages, pyocins, PLTS and T6SS. The nomenclature is based on the minimal phage tail [1]. PLTS and T6SS are additionally accompanied by an AAA+ ATPase, which facilitates sheath recycling in case of the T6SS. The asymmetric unit of the contractile T6SS sheath consists of a gp18-like sheath protein VipB (blue) and an additional protein, VipA (red).

Table 1. Structural and functional communalities and differences between contractile phage-like systems.

	minimal phage	R-Type	T6SS	PLTS
baseplate hub/spike	+	+	+	+
spike with effector domains	+/-	-	+	-
PAAR proteins	+	?	+	+
tube initiator	+	+	?	?
sheath initiator	+	+	+	+
other baseplate proteins	+	+	-	+
tail fiber	+	+	-	+
tail tube	+	+	+	+
tail sheath core (gp18 domain III and IV), strand exchange	+	+	+	+
tail sheath modifications	protease-resistant fragment (PRF)	-	recycling domain	?
tape measure protein	+	?	?	+
tube terminator	+	?	?	+
sheath terminator	+	?	?	?
AAA+ ATPase (function)	-	-	ClpV (recycling)	Afp15 (assembly)
substrate	DNA	H^+/ions	protein	protein (?)
released	host lysis	host lysis	intracellular	host lysis

Summarizing the available structural data, Leiman and Shneider describe a theoretical "simplest contractile tail-like structure" [1] comparing T4 phages, P2 phages and others (see also table 5.3 in [1]): a trimer of gp27 assembles around a gp5 trimer. Together they form the so-called baseplate hub. Concentric hexagonal layers of six gp25, six gp6 dimers, and six proteins orthologous to

gp53/gp7 surround the hub, completing the minimal baseplate. The tail fibers are attached to the baseplate. For polymerization of the tube, a tail tube initiator consisting of proteins gp54 and possibly also gp48 forms upon the gp27 trimer. Hexameric gp19 rings build up the tail tube and the tail sheath (gp18) wraps in six right-handed helical protofilaments around it. A tape measure protein with an elongated helical conformation interacts with the tube (gp3) and sheath (gp15) terminator complex and determines the length of the tail.

1.2. R-Type pyocins

Pyocins have been first described in *Pseudomonas aeruginosa* as antibacterial agents by Jacob in 1954 [31]. They are divided into three classes based on their morphology: rod-like R-type, flexuous rod-like F-type and soluble S-Type pyocins [2]. F-Type pyocins, which have been characterized for the first time in 1967, are related to the non-contractile λ phage while R-type pyocins are related to the *Myoviridae* P2 phage [23,32]. The latter ones form 1200 Å long and 180 Å wide filled rods, which occur also in a contracted form with an ejected core and a hollow sheath [11,33]. The contracted sheath is 460 Å long and 240 Å wide. A 240 Å-diameter baseplate structure is attached to the sheath and contraction can be induced under acidic or basic conditions or when treated with 6 M urea [11,33].

Pyocin gene clusters are present in the genomes of *P. aeruginosa* and other gram-negative but also gram-positive bacteria [34–37]. The R2 pyocin genes are organized in a cluster together with genes encoding the F2 pyocin [23]. The R2 specific region comprises 16 genes of which 12 are homologous to contractile bacteriophage genes including genes coding baseplate proteins (gp6, gp25, gp27, gp53), tail fiber proteins, the tail tube protein (gp19), the tail spike protein (gp5) and the contractile sheath protein (gp18) (Figure 1 B). Additionally, genes controlling the formation of tail and fibers and genes causing lysis are included in the cluster. Its expression can be activated via RecA upon DNA damage caused e.g. by UV irradiation or mitomycin C [38]. Once expression of pyocin genes is induced, one bacterial cell produces up to 200 pyocin particles, which are released by lysis [39]. Similar to target recognition in bacteriophages, the tail fibers of pyocins recognize bacterial membrane receptors [39,40]. When attached to their bacterial target, they contract and kill the cell by forming a permanent channel across the membranes. As a consequence the membrane potential is lost and active transport inhibited [41,42]. Pyocins are highly potent toxins as one pyocin particle is sufficient to kill a bacterium [1]. Usually, *P. aeruginosa* strains are resistant to their own pyocins [43].

1.3. Phage-like protein translocation structures

Recently, other phage-like structures related to the P2 phage tail in gram-negative and gram-positive bacteria, as well as in Archaea have been summarized in the PLTS (phage-like protein translocation structures) cluster comprising 13–16 core genes [3]. The cluster is phylogenetically distinct from other contractile systems employed by bacteria. Yet, it is functionally related to the T6SS as it encodes also for PAAR repeat proteins and an AAA+ ATPase. These similarities led to the hypothesis, that PLTS are involved in translocation [3]. Furthermore, the cluster contains a LysM-like peptidoglycan-binding protein but no lysis system like seen in pyocins and phages. However, scarce experimental evidence suggests that they are released by host cell lysis [3,17]. The anti-feeding prophage (Afp) in *Serratia entomophila* and its homologue in the *Photorhabdus*

virulence cassette (PVC) belong to the PLTS group [3]. Both are pyocin-like contractile machines, which are secreted and directed against insects [1,44]. PVC leads to actin cytoskeleton rearrangements in insect and mammalian haemocytes, while up to date Afp has only been found to act on the New Zealand grass grub *Costelytra zealandica* leading to cessation of feeding in larvae [45,46].

The afp gene cluster encodes for three tail sheath orthologues with sizes between 40 and 50 kDa, two tail tube orthologues, and orthologues to baseplate proteins, a terminator protein, and additionally, an AAA+ ATPase which distinguishes the PLTS cluster most from pyocins and phages [3,16,45,46,47] (Figure 1 B). Interestingly, in the C-terminal region all three sheath proteins show approximately ~40% sequence similarity to the T4 tail sheath protein gp18 [16]. The *S. entomophila* anti-feeding prophage has also been characterized biochemically and by electron microscopy. Elongated Afp particles are approximately 1000 Å long and their sheath has a diameter of approximately 200 Å. The diameter of the baseplate is about 300 Å [16]. The Afp15 AAA+ ATPase is absolutely necessary for formation of a structure consisting of some baseplate proteins and the needle. This structure however lacks some putative baseplate proteins, the sheath protein, and toxin associated proteins [47]. One might therefore speculate that the AAA+ ATPase is involved in the assembly of baseplate and needle. In the absence of the terminator protein Afp16, the baseplate and the tail tube of the particle but no sheath can be formed. C-terminal truncation of the terminator protein leads to variations in the length of the Afp particle and infrequently also to incomplete sheath formation or association of a contracted sheath with the apical end of the tubule [47]. Recently, Afp14 was found to be a tape measure protein [48]. Finally, the tail sheath contains stoichiometric amounts of the two major tail sheath proteins Afp2 and Afp3, while a third protein, Afp4, is present in a smaller amount [47].

The so-called metamorphosis-associated contractile structures (MACs) have been found lately in *Pseudoalteromonas luteoviolacea* [17]. They resemble pyocins in so far that they are released by cell lysis, but differ by the formation of huge hexameric, intracellular arrays in the host cell, which are connected by their tail fibers. MACs can induce metamorphosis in marine tubeworms by an unknown mechanism. They possess just one tail sheath protein of around 62 kDa [17]. Other phage-like structures which are released by lysis and form hexameric arrays have also been described in *Streptomycetes endus* [49].

1.4. Type VI secretion system

The T6SS has been first described in 2006 [50,51]. It is a bacterial secretion system used to inject toxic effectors into competing bacterial cells and also eukaryotic cells. The T6SS consists of 13 core elements *tss A-M (type six secretion A-M)* encoded in a cluster which can be found in about 25% of all known genomes of gram-negative bacteria, mostly proteobacteria [52,53]. T6S loci are sub-classified phylogenetically into a main proteobacterial (T6S^{I}), the *Francisella* (T6S^{II}) and the Bacteroidetes cluster (T6S^{III}). No homologues of TssE, TssG, TssJ and TssH have been found in T6S^{II}, and TssA, TssJ, TssM and TssL have not been found in the T6S^{III} [52–56]. Since T6S^{I} is the best characterized system, we focus on the proteobacterial cluster in this review. The T6S locus can be divided into genes *tssA-I*, that encode for proteins forming a contractile, phage-tail-like structure and *tssJ-M* that encode membrane proteins [22,53]. Additionally, there is a set of *tss-associated genes (tag) A-P* which are involved in the regulation of secretion or in the case of tagJ in the recycling of

the contractile tubule (see section 2.) [21,57].

The phage tail-like sub-complex comprises one or more orthologues for the gp19 tail tube protein TssD/Hcp, a fusion of baseplate hub protein gp27 and tail tip protein gp5 called TssI/VgrG and the gp25 baseplate protein homologue TssE [58,59,60]. The contractile sheath is formed by two proteins, TssB/VipA and TssC/VipB [12,61]. VipA and VipB form a dimeric protomer, which is composed of 3 domains formed by both peptide chains together. The innermost 2 domains composed the first 70 amino acids of VipA and residues 95-492 of VipB are structurally homologous to gp18 [13,14,15,62]. So far no structural or functional data is available for TssA, TssF and TssG. The AAA+ ATPase ClpV/TssH also belongs to the core elements of phage-tail like sub complex. Even though it is not essential for T6S, impairment of ClpV leads to a 90% loss of T6SS-mediated antibacterial activity [12,63] as it facilitates recycling and reuse of essential system components. The phage tail-like complex is putatively attached to the membrane complex via the cytoplasmic protein TssK [64]. Surprisingly, no protein of the T6SS membrane complex bears homology to bacteriophages, but inner membrane proteins TssL and TssM are structurally homologous to DotU and IcmF of the *Legionella* Type IV secretion system [65–68]. TssJ is a lipoprotein anchored in the outer membrane [69]. It oligomerizes *in vivo* and interacts with TssM, while TssM forms multimeric complexes that interact in the inner membrane with TssL [67,69,70]. Thus, it was suggested that all T6SS membrane proteins assemble into a channel-like structure spanning the periplasm [22].

2. The Type VI Secretion System: Regulation and Function

The Type VI secretion system is regulated on a transcriptional and posttranslational level. In this review, we concentrate on two examples: transcriptional regulation by VasH and post-translational control by the PpkA/PppA signaling cascade. T6SS regulation has been reviewed elsewhere [20,21,71]. VasH is a σ^{54} dependent transcriptional activator /bacterial enhancer binding protein (bEBP) of T6SS expression in *V. cholerae*, which is essential for T6SS-mediated killing of amoeba and bacteria [51,63,72,73]. It consists of N-terminal activator domain, a central domain with Walker A/B motifs and a C-terminal HTH domain. The latter two were found to be essential whereas deletion of the activator domain could be tolerated [73]. VasH showed autophosphorylation *in vitro* which is characteristic for other bEBPs and suggests that VasH might be a downstream target of a sensor kinase [72]. Yet, it is somewhat disputed whether VasH acts upon the main T6SS gene cluster or only upon the *hcp* operons [21,72,74].

The T6SS acts in cycles of secretion apparatus assembly, contraction and secretion apparatus disassembly (Figure 2), which are suggested to be regulated by a signaling cascade involving TagQ/R/S/T, the serine/threonine kinase TagE/PpkA, its antagonist phosphatase TagF/PppA as well as TagH/Fha in *Pseudomonas aeruginosa* (Figure 2 A) [21,75]. It is not known, whether the T6SS cascade is initiated by only one stimulus or several events. However, membrane rupture caused by either Type IV secretion system mediated conjugation, polymyxin B or a T6SS attack by another bacterium triggers a T6SS response [75,76,77]. The *P. aeruginosa* counterattack towards a *V. cholerae* T6SS attack causing membrane rupture is conducted in a TagT-dependent, spatial and temporal manner targeting the insulting bacterium. Interestingly, TagQRST are not essential for T6SS function [78], suggesting that so far unidentified regulatory proteins might be involved in T6SS dueling. Also, not all T6SS are associated with a PpkA/PppA system [21]. Generally, T6SS formation and activity is dependent on phosphorylation of Fha1 (forkhead-associated 1) by TagE/ PpkA while

Fha1 dephosphorylation by TagF/PppA inhibits T6SS activity. Consequently, deletion of Fha1 abolishes T6SS apparatus formation altogether [79,80]. TagE/PpkA is dependent on the presence of the periplasmic protein TagR and outer membrane lipoprotein TagQ, to which TagR is associated [81,82,83]. Additionally, a complex in the inner membrane consisting of transmembrane protein TagS and the ATPase TagT is needed for TagE/PpkA activation [83]. Interestingly, PpkA also directly phosphorylates baseplate complex protein TssL in *Agrobacterium tumefaciens*. The phosphorylated protein then binds Fha1 and triggers a conformational change of the baseplate complex protein TssM, which enhances Hcp recruitment to TssL [84]. Furthermore, TssM can bind and hydrolyze ATP causing a conformational switch that facilitates TssM-TssL-Hcp complex formation. It should be noted that ATP-binding is not essential in every species [67,85,86] (Figure 2 B).

The baseplate/tube tip protein VgrG and a PAAR protein sharpening the tip must be present for T6S secretion, presumably as a starting point for the needle complex assembly [87,88]. The needle complex functions as a template for proper assembly of the elongated sheath [80,88].
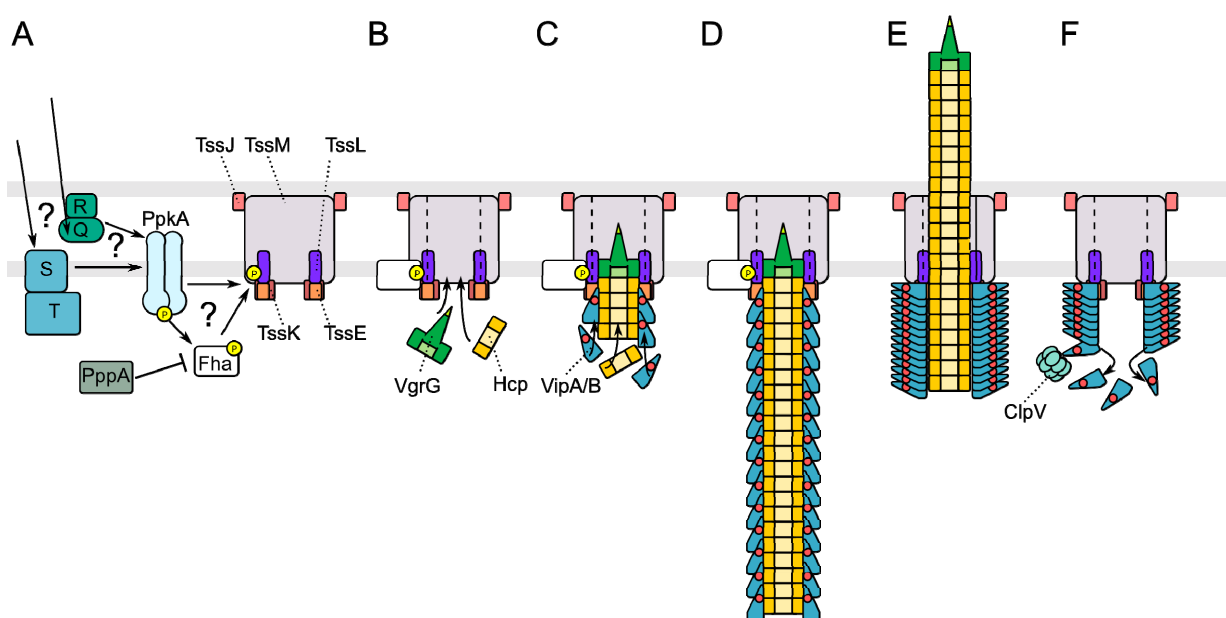

Figure 2. Model for Type VI secretion. (A) Activation of the PpkA/PppA-Fha signaling cascade leads to phosphorylation of TssL and binding of Fha. Signals are possibly integrated via TagQ(Q)/TagR(R) and/or TagS(S)/TagT(T) which trigger autophosphorylation of PpkA (inhibited by PppA). PpkA phosphorylates Fha and/or TssL. (B) Binding of Fha to TssL activates ATP hydrolysis in TssM thereby inducing a conformational change and recruitment of the baseplate/needle tip complex VgrG/PAAR as well as the needle tube protein Hcp to the baseplate complex. (C) The needle complex and the surrounding VipA/B sheath are assembled in a coordinated manner. (D) The loaded complex is ready for contraction. (E) Contraction of the VipA/B sheath leads to ejection of the needle complex. (F) The AAA+ ATPase ClpV disassembles the contracted sheath for recycling. The color code is as in Figure 1 B.

Furthermore, in analogy to the T4 phage tail, the gp25 homologue TssE might function as a primer [1,60]. The two sheath proteins VipA and VipB are most likely being incorporated into the tubule as a dimer as individually expressed proteins are unstable [61,89,90]. The loaded complex is thought to be formed in a coordinated fashion where Hcp hexamers are included into the complex shortly before VipA/B protomers are recruited to the same layer of the growing complex [22,91] (Figure 2 C, D). The growing needle and the baseplate would therefore act as a template for the elongated form of the sheath [11,92]. No tape measure proteins or tail terminator proteins are known for the T6SS.

The contraction of the sheath leads to ejection of the needle (Figure 3 E). According to the Multiple Effector tRanslocation VgrG model (MERV) effectors are presumably translocated via the needle complex [87]. The Hcp hexamer has an inner diameter of 40 Å, enough to accommodate small folded or large partially unfolded proteins. Putative effector proteins can be co-immuno-precipitated with Hcp in *E. tarda* [50,85]. Silverman *et al.* showed in 2013 that Hcp could act as chaperone and substrate receptor for T6SS effectors [93]. Furthermore, PAAR proteins forming the very tip of the T6SS needle can either carry additional effector domains such as nucleases or peptidases or interact with other effectors [87]. Moreover, the tail tip protein VgrG can be functionalized with a C-terminal effector domain, e. g. VgrG1 of *V. cholerae* with a actin crosslinking domain (ACD) or VgrG3 with a peptidoglycan hydrolase domain [51,94]. Both VgrG1 and VgrG3 are secreted by the same T6SS, which raises the question of specificity for a certain cell type. The ACD is clearly directed against eukaryotic cells while the peptidoglycan hydrolase mostly targets prokaryotes. Brooks *et al.* speculated that VgrG3 might assist *V. cholerae* in penetrating the mucosal layer of the intestine and a delivery of both effectors by the same secretion system seems efficient [94].

The T6SS trigger mechanism for contraction remains to be elucidated. In bacteriophages, attachment of the tail fibers leads to a major rearrangement of the baseplate, which is then transduced to the sheath. However, apart from TssE there are no known homologies of the T6SS membrane complex to the viral baseplate. Presumably, at least TssM and TssL might undergo a similar structural transition before transmitting the signal further to the tubule. As far as it is known to date, the membrane complex does not cross the outer membrane, it is therefore unlikely that the T6SS complex itself initiates contraction. Albeit signaling cascades such as the one described above could target the T6S membrane complex to trigger secretion.

Upon contraction, the AAA+ ATPase ClpV is recruited to the T6SS tubule via a special binding motif on VipB to disassemble the VipA/B tubule under ATP consumption [12,61,80,95]. Alternative disassembly pathways mediated by TagJ and VipA homologues have also been suggested in a subset of T6SS. Here, TagJ binds to the N-terminus of VipA, and also interacts with ClpV. TagJ might therefore act as a recruitment platform for the ATPase [96]. It is not known yet, whether VipA/B protomers are recycled to build new, loaded T6S tubules or whether VipA and VipB are completely unfolded or degraded. Considering that more than one T6SS tubule is formed in a cell and that VipA/B protomers are quickly reassembled after the tubule is taken apart by ClpV, a recycling of protomers is certainly more efficient than a constant *de novo* synthesis of the proteins [12,61,76].

3. Structural Homologies in the Contractile Machinery

As outlined above, contractile phage tail-like structures consist of several building blocks with

structural homologs present in various contractile systems: the baseplate hub/spike, the needle, the sheath and the sheath initiator. In this section, we summarize the structural knowledge about these proteins and describe how they differ from each other. Potentially homologous proteins that have not been identified in all systems are the tail tube initiator, the tube and sheath terminator proteins, as well as the tape measure proteins. Initiator and terminator proteins have been found to be essential for contractile phages [92,97] and a sheath terminator protein has also been identified for a PLTS [47]. Tape measure proteins control the length of the tail in bacteriophage and PLTS [48,98].

The baseplate hub/spike complex consisting of gp27 and gp5 has been crystallized [99]. Three gp27 proteins and three gp5 proteins form a heterohexameric complex. Gp27 consists of 4 domains, of which the first and the third domain are a pair of β barrels. In the gp27 trimer, the β barrels describe a pseudohexameric outline, thereby bridging the symmetry mismatch between the hexameric needle plus baseplate and the trimeric spike. The remaining two domains interact with the N-terminal oligonucleotide/oligosaccharide-binding (OB) β barrel domain of gp5. A central lysozyme domain, and a C-terminal domain, which forms the three-stranded β-helix in the spike complex, follows the OB domain of gp5. During maturation, the linker between the central and C-terminal domain that blocks the substrate recognition pocket of the lysozyme domain is cleaved [100]. Activated lysozyme is suggested to hydrolyze the peptidoglycan layer during infection. Nevertheless, gp5 orthologue of several phages miss the lysozyme domain and in some cases it is attached to the tape measure protein or the gp27 orthologue [1]. Full lysozyme activity is not essential for infection, as T4 phages with residual lysozyme activity of 10 % are still infectious under lab conditions [1,100]. In the T6SS, the spike protein VgrG is a structural homolog of a fusion between gp27 and gp5. The lysozyme domain, which is present in gp5, is missing in VgrG [58]. In some cases, additional effector domains are attached to the C-terminal β helix of the VgrG spike [101–104]. For example, VgrG1 of *Vibrio cholerae* extends into an actin-crosslinking domain, which acts upon the G-actin subunits of the eukaryotic actin cytoskeleton [104]. A gp27-gp5 nonameric complex lacking the lysozyme domains could also be accommodated in the densities representing the spike of the anti-feeding prophage EM reconstruction [16]. The tip of the VgrG β helix is sharpened by a zinc ion-coordinating, PAAR repeat protein, which is also found in the T4 phage [87]. In contrast, the spike of bacteriophages P2 and φ92 is sharpened by an additional C-terminal apex domain of the β helix that coordinates an iron atom [105].

The needle itself is built up from hexameric rings of gp19/Hcp proteins [50,58,59]. Hcp oligomerizes into hexameric rings of 100 Å diameter *in vitro* forming a 24-stranded β-barrel on the inside. The inner diameter of around 40 Å is sufficient to hold small, folded or large, unfolded proteins or dsDNA [50,106]. Interestingly, some bacteriophage tail tube proteins such as gpV do not hexamerize, but readily assemble into tubes [59]. The T4 phage needle protein gp19 needs the presence of baseplate complexes [107] or dissociated tube complexes [108] in order to oligomerize into tubes. *P. aeruginosa* Hcp3 hexamers only form short needles *in vitro* [58]. Binding between Hcp rings is weak; the k_D was measured to be approximately 7 μM [109]. Even though the overall structure is conserved, the inner tubule wall is adapted to its substrate: the pyocin needle tube conducts protons or ions and is therefore negatively charged on the inside, while phage needles translocate negative-charged DNA inside a positively charged tube, and Hcp possesses a neutral inner wall to transport proteins [11]. Hcp directly interacts with VgrG-1 in *A. tumefaciens* [110]. Yet in bacteriophage T4, gp19 assembles into the tail tube upon presence of tail tube initiator proteins gp48 and gp54 [111]. In R-type pyocins of *P. aeruginosa*, a homologue to the putative phage P2 tube
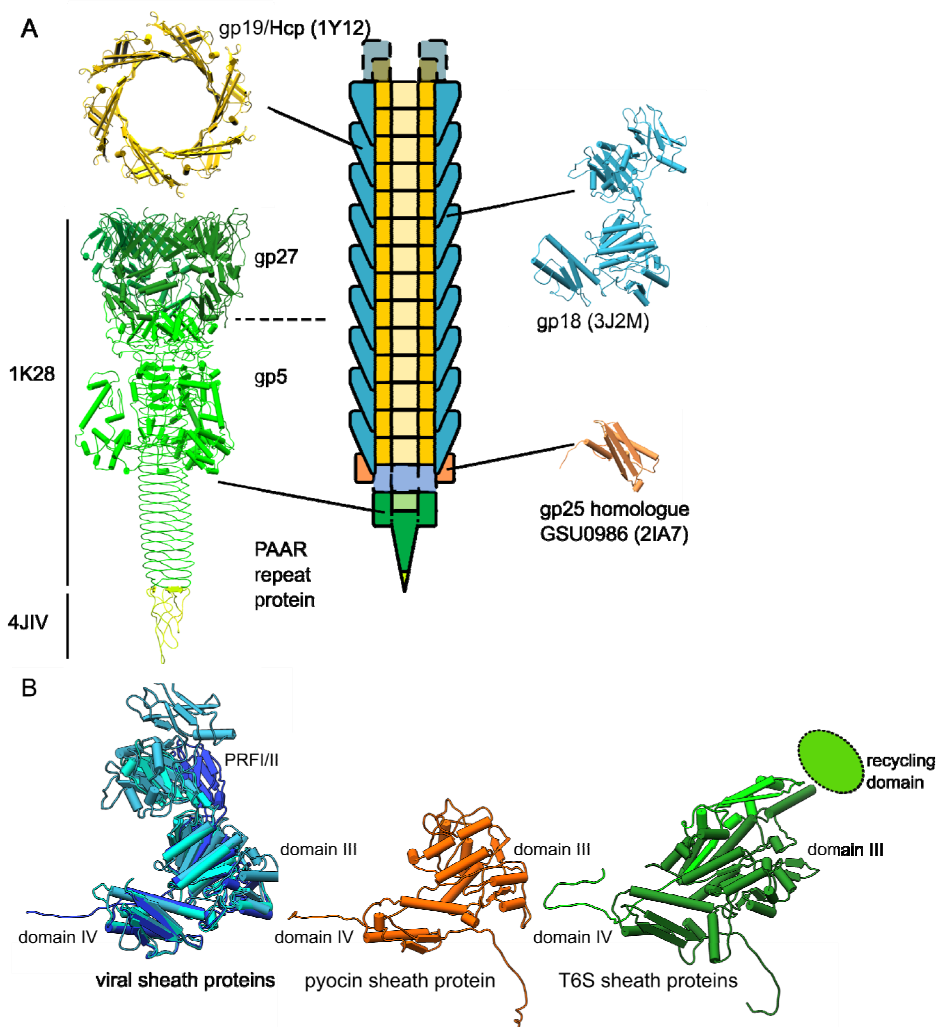
Figure 3. Homologous proteins shared between all contractile phage-tail like assemblies. (A) Hexameric rings of gp19/Hcp or their homologs form the needle complex (pdb-id: 1Y12). The needle complex is spearheaded by gp27 and gp5, which occur in the structurally homologous fusion protein VgrG in the T6SS. Gp27 and gp5 have been co-crystallized (pdb-id: 1K28). The beta-helical C-terminal domain of gp5 is sharpened by a PAAR repeat protein (pdb-id: 4JIV). The needle complex is surrounded by the contractile sheath, which consists of six helical protofilaments formed by gp18-like proteins (pdb-id: 3J2M). The baseplate protein gp25 putatively acts as a sheath initiator protein (pdb-id: 2IA7). (B) *Left:* Crystal structures of viral tail sheath proteins gp18 (light blue, pdb-id: 3J2M), DSY3957 (blue, pdb-id: 3HXL) and Lin1278 (cyan, pdb-id: 3LML) are overlaid. They reveal the greatest extent of structural homology in domains III and IV. *Middle:* the tail sheath protein of R2 pyocin (orange, pdb-id 3J9R) demonstrates a similar architecture in domains III and IV, PRF domains are missing. *Right:* the TssB/C (light green/dark green) is also structurally conserved in domains III and IV, but is extended by a TssB/C recycling domain, for which no high resolution structure is available yet (pdb-id 3J9G).

initiator protein has been described [1,23]. Cysteine-crosslinking indicated that EAEC Hcp1 rings stack head-to-tail into longer tubes *in vivo* [88]. This also implies, that the needle complex likely does not follow the helical symmetry of the sheath. However, X-ray diffraction studies of isolated T2L tail tubes, an EM reconstruction of sheath formation impaired Afp particles and well resolved one-to-one contacts between the sheath and tube subunits in the helical reconstruction of the φRSL1 phage tail suggests the opposite [7,16,106]. The recently published cryo EM reconstruction of the R2 pyocin clearly shows, that the tube follows the helical symmetry of the sheath in the elongated state [7,11,16,106]. Here, one-to-one contacts are formed between complementary charged patches on the most C-terminal helix of the sheath protomer and the needle tube subunit [11]. For the T6SS needle of *E. tarda*, it has been shown that a conserved set of positively charged residues at the C-terminus as well as three negatively charged residues at the N-terminus of Hcp1 are important for the function of the system.

It has been suggested, that also the assembly of the pyocin needle is directed by complementary charges at the ring interfaces [11]. Additionally, a loop between strands 2 and 3 of *Burkholderia pseudomallei* is involved in Hcp ring interaction; the corresponding loop in the pyocin homologue is located at the interface between hexamers [11,112]. Co- immuno- precipitation as well as bacterial two-hybrid experiments also indicated an interaction between the tube protein and the surrounding sheath via VipA [88,113].

The T4 tail sheath protein gp18 consists of 4 domains, which are inserted into each other in a matrioshka-like manner with domain IV representing the "outer" and domain I the "innermost layer" —a domain architecture, which is also conserved in other tail sheath proteins (Figure 3 B) [1,9,114]. A fragment comprising domains I-III (gp18M) has been crystallized and domain IV has been modeled on basis of the homologous tail sheath protein LIN1278 [9,114,115]. β sheet-rich domains I and II form a protease-resistant fragment (PRF). Domain I in the first layer of the sheath is in contact with the baseplate in the elongated state hinting towards a role in sheath assembly or even contraction [114], domain II-III provide energy for the contraction by creating new inter-subunit contacts and domain IV maintains the sheath connectivity during the contraction process [114]. In a crystal structure of another tail sheath protein DSY3957, the first 25 N-terminal residues form a β strand, which is swapped to the β sheet in domain IV of the symmetry-related molecule in the crystal. This led to the hypothesis that protomers within a protofilament are inter-connected by a "chain-swapping" mechanism [1]. Recent high-resolution cryo EM reconstructions of the contracted T6SS tubule of *F. novicida* and *V. cholerae*, and of the R2 pyocin revealed that the protomers are indeed interconnected [11,14,15]. The C-terminus of both, VipB and the pyocin sheath protein, reaches across to the C-terminal domain of the preceeding protomer of the same protofilament. The N-terminus of VipA and likewise the pyocin sheath protein similarly link to the C-terminal domain of the neighboring protomer in the ring.

The PRF is missing in the VipA/B protomer, yet the first 70 amino acids of VipA and residues 95-492 of VipB fold into two domains that share a structural homology to gp18 domains III and IV [11,13,14,15,62,114]. Hence, the viral tail sheath protein has been split up into two proteins. It is noteworthy that in the T6S locus *vipa* generally directly precedes *vipb* [53] and in some cases the sequences are even fused together such as in *Hylemonella gracilis*, *Burkholderia glumae* or as in the γ proteobacterium HdN1 [62]. The C-terminus of VipA and the N-terminus of VipB form a T6SS-specific recycling domain, which harbors the binding site for the AAA+ ATPase ClpV on VipB. Unlike the PRF domains, which possibly protect the virus sheath in the contracted and elongated

state from extracellular proteases, the ClpV binding site should only be accessible after T6SS contraction. The different orientation of the outer domains in the helical assembly is due to the almost triangular outline of the TssB/C protomer compared to the S-shaped conformation of gp18 (Figure 3B) [13,80,95]. According to two-hybrid data, the interaction between VipA and VipB is conserved across species boundaries and is mainly mediated by a long α helical region in VipA [89,116,117]. Impairing this interaction leads to a reduced stability of VipB and loss of T6S function [89]. Additionally, the formation of a large six-stranded β sheet between VipA and VipB in domain III stabilizes the protomer [15]. The VipB C-terminal domain homologous to Domain IV is essential for sheath polymerization in the Type VI secretion system [13,62]. Also, deletion of the swapped β strand impairs T6SS assembly in *V. cholerae* but not in *F. novicida* and both swapped strands of VipA and VipB are essential for secretion [14,15]. The polymerization property of sheath protein gp18 has been investigated in C-terminal truncation mutants. Here, the polymerization depends on a polypeptide stretch from residues 507 and 530 [114,118]. Truncation by up to 129 residues from the C-terminus leads to sheath formation in a contracted or "over-contracted" state while deletion of more residues resulted in either complete loss of polymerization (when the loop sequence was still partially present) or in formation of tubules reminiscent of so-called "transitional helices"/partially contracted sheaths (when up to 248 residues are deleted from the C-terminus) [118,119]. Gp18 mutants also polymerized when this stretch was partially deleted while domain IV was still present [120]. Additionally, single mutations in an α helical region ranging from 578 aa to 599 aa in domain IV demonstrated to either impair the interaction with the baseplate, to destabilize the elongated state, or to lead to pH- or ionic strength-dependent depolymerization of the sheath [121].

Gp25 is the most conserved protein in the baseplate of T4 phages and other phages and it is homologous to TssE in the Type VI secretion system [1,58,60,122]. It yet has to be characterized in bacteriophages. However, the gp25-like protein GSU0986, which is encoded in a prophage region of *Geobacter sulfurreducens,* has been crystallized and used for homology modeling of *P. aeruginosa* TssE [60]. It shows a three-stranded anti-parallel β sheet with two long anti-parallel α helices, a long loop region and a third smaller α helix attached to the core structure. A glutamate in a conserved EPRL motif is essential for T6S [60]. Due to its localization in the baseplate and its structural similarity to domain IV of tail sheath proteins, it has been proposed to act as an initiator for sheath polymerization [1].

4. Cryo-EM Reconstructions of Contractile Machines

Most cryo-EM reconstructions of contractile phage-like systems have been obtained from bacteriophages. Despite available phage tail structures of φKZ [8,9] and φ92 [10], in this review we only elaborate on the best-characterized system of bacteriophage T4 [5,6] and the so far best resolved tail of bacteriophage φRSL1 [7]. We compare these structures to a reconstruction of a pyocin [11], a PLTS [16] and a T6SS [15]. Reconstructions of different conformational states —an elongated and a contracted one—have only been obtained for the T4 phage and the R2 pyocin, while the PLTS *S. entomophila* anti-feeding prophage has only been resolved in its elongated state.

Known contractile phage tail-like machines share a common architecture. It can either be described as six filaments forming a right-handed superhelix or according to the historic descriptions of coliphage tails as a stack of hexameric rings (annuli) rotated against each other (e.g. [123]).

Reconstructed contractile tails consist of 114 (φRSL1) to 264 (φKZ) subunits. However, there are also shorter tails known containing only about 90 subunits [1,124]. Generally, the arrangement of subunits in the extended and the contracted states is very similar (see Table 1). In the extended state, the unit rise of the helical array ranges from 36.7 Å for the phage φKZ [8,9] to 40.6 Å of bacteriophage T4 [6], while the unit twist ranges from 17.2° [6] of T4 to 22° for phages φKZ [8] and φRSL1 [7]. After contraction the subunit rise lowers to a distance between 16.2 (R2 pyocin) [11] to 21.8 Å (VipA/B tubule) [15], while the subunit twist extends to an angle ranging from 26.6° (*F. novicida* T6SS tubule) [11] to 34.1° (φKZ phage) [9].

The extended state of the T4 phage tail has been resolved to 15 Å. The 925-Å long tail consists of 6 protofilaments of 23 subunits each. The outer diameter of the sheath is 240 Å holding a 95 Å wide tail tube. The contact area between sheath and tube was found to be rather small (200 Å^2 at density threshold of 1 σ) [6]. Rigid-body fits of gp18 into the map showed that domains II-IV maintain inter-protofilament and intra-protofilament contacts while domain I of the tail sheath protein forms the protruding cogs [6,114]. The contractile sheath of phage φRSL1 is slightly shorter (720 Å), but otherwise resembles the T4 sheath architecture. The φRSL1 tail sheath consists of six protofilaments each comprising 19 protomers [7]. A section of the elongated tail has been reconstructed to 9 Å resolution employing helical symmetry. The density of the map accommodates gp18 PRFI, PRFII and domain III (12%, 13% and 29% sequence identity to φRSL1 tail sheath protein), even though the relative domain orientation especially of PRFI relative to PRFII differs from that of the gp18 crystal structure [7]. As in the elongated T4 sheath, the architecture is maintained by contacts between domains II-IV. Additionally, there is also a peripheral inter-protofilament contact between domain IV and domain I [7]. Contacts between the sheath and tail tube are well defined, yet the interpretation was ambiguous as a full-length model of gp18 was not available at the time. Therefore it was unclear, whether an unfilled α helical density at the tube/sheath interface belongs to domain IV of the sheath or is an additional protein [7].

The elongated state of the R2 pyocin has been resolved at 3.5 Å resolution, which allows for *de novo* chain tracing [11]. The reconstruction also includes the inner tube, which has the same helical symmetry as the surrounding sheath but has a featureless surface while the sheath demonstrates prominent right-handed helical ridges. The pyocin sheath protein consists of only two domains homologous to domains III and IV of gp18 with the N-terminal, "swapped" arm stretching out along two preceeding protomers of the same protofilament. In this reconstruction, also the interface between sheath and tube could be analyzed for the first time in molecular detail. The most C-terminal helix in domain IV appears to interact with the needle, possibly pushing it forward upon contraction. Despite a uniform length of pyocin tubules, there is no additional density corresponding to a tape measure protein inside the needle, although symmetrization could cause the densities for the tape measure protein to be lost.

At first sight, the architecture of the sheath in the EM reconstruction of the elongated Afp particle differs clearly from the other contractile machineries, as the helical geometry is described by parameters twice the size of other phage tail like structures [16]. However, the contractile sheath consists of at least two (Afp2/3) of the three sheath proteins encoded by the locus and all sheath proteins share a ~25% sequence identity to the C-terminal region of gp18 [16,47]. The authors have noted that the sheath is composed of a series of double-layered discs rotated against each other by 40.5°. The height of one half-layer agrees very well with the dimensions of gp18 domain IV of approximately 4 nm and the average subunit rise of 3.5–4 nm of a contractile phage tail. Thus, two of

three sheath proteins can be accommodated in the density of the sheaths asymmetric unit [16]. It is therefore tempting to speculate that the Afp contractile sheath consists of alternating homohexameric rings of sheath proteins Afp2 and Afp3.

The contracted T4 phage has been resolved to 17 Å [5]. After contraction, the sheath is reduced to a length of 420 Å and widened to an outer diameter of 330 Å. The sheath completely detaches from the tail tube and has a new inner diameter of 150 Å. The gp18 crystal structure can be placed into the EM density as a rigid body. Protomers of consecutive annuli are interdigitated, giving it a 12-meric cog wheel-like appearance, when looked at from above. Contact areas between domains PRFII and domains III of neighboring protomers are 5 times increased, while domain IV - domain IV contacts remain unchanged [114]. Polysheath complexes of gp18 resemble very much the contracted state of the native phage tail [125].
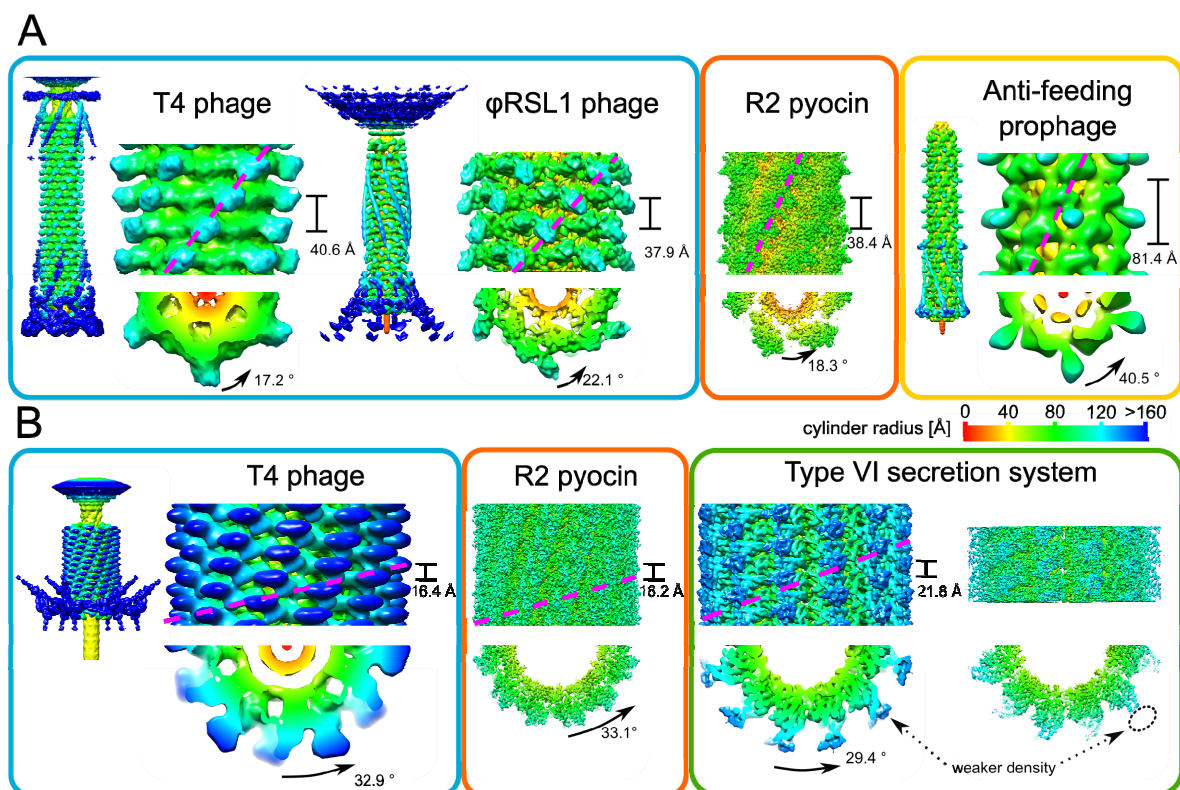

Figure 4. Electron microscopic reconstructions of contractile phage-like structures. (A) Reconstructions of elongated structures of contractile bacteriophages (T4 phage (EMD-1126) and φRSL1 phage (EMD-2245 and EMD-2244)), the R2 pyocin (EMD-6270), and the PLTS cluster (*Serratia entomophila* anti-feeding prophage (EMD-2419)) are shown in side (*above*) and top views (*below*). (B) Reconstructions of contracted structures of bacteriophages (T4 phage (EMD-1086)), the R2 pyocin (EMD-6271), and the T6S system (EMD-2524 and EMD-2699) also presented in side (above) and top views (below). One protofilament in each sheath structure is indicated (magenta) and unit rise and twist are given. The EM maps are rendered at their recommended threshold and colored according to the radial distance from their rotational symmetry axis. The structures are grouped according to the classification described in Figure 1 as indicated by colored boxes.

The contracted R2 pyocin sheath has been reconstructed to a similar resolution as the elongated state [11]. Comparison of the derived atomic models shows, that contraction involves only rigid-body movements of the protomers with an increase in contact area with the formation of new charge pairs as compared to the elongated state. The needle itself could not be resolved in the reconstruction, as it does not undergo the same structural transitions as the sheath during contraction and therefore its helical symmetry most likely still resembles the elongated state.

The contracted T6SS sheath has been reconstructed at 3.2–4.0 Å resolution [15]. It is 290 Å wide with an inner diameter of 110 Å. Even though the tubule demonstrates left-handed helical ridges due to a subunit twist of less than 30° the architecture is very similar to other contractile structures. The C-terminal and middle domain of VipB which are structurally homologous to domains III and IV of gp18 form most of the contacts in the tubule, protofilament connectivity is mainly maintained by contacts between C-terminal domains of VipB and the swapped β strands from neighboring subunits. The helical ridges are formed by the protruding cogs, which hold the unique VipB recycling domain. This domain has been resolved in a cryo EM reconstruction of a polysheath sample with otherwise similar architecture [13], showing mainly α helical features. The high-resolution structure of contracted T6SS tubule from *F. novicida* shows a lower helical rise and turn [14]. However, comparison of helical parameters of the various contractile phage-like systems demonstrates, that even though the underlying structural features of the protomers are rather conserved, the overall architecture of the sheath reveals some variability (Table 2).

Table 2. Comparison of contractile sheaths.

	T4		φ KZ		φ RSL1	R2 pyocin		Afp *S. m.*	T6SS *V. c.*	T6SS *F. n.*
state (el./con.)	el. [6]	con. [5]	el. [9]	con. [9]	el. [7]	el. [11]	con. [11]	el. [16]	con. [15]	con. [14]
unit rise [Å]	40.6	16.4	36.7	17.9	37.9	38.4	16.2	81.4	21.8	20.8
unit twist [°]	17.2	32.9	22	34.1	22.1	18.3	33.1	40.5	29.4	26.6*
outer diameter [Å]	240	330	120	160	245	180	240	230	290	240
inner diameter [Å]	100	150	260	315	100	85	110	90	110	120
MW gp18-like protein [kDa]	71.3		77.6		68.5	41.2		38.8/48.7/45.5	55.6	57.9
MW other sheath proteins [kDa]	-		-		-	-		-	18.5	21.0

* adapted to fit the helical array of the other systems

5.   Towards a Model for Contraction

The presented similarities in sheath architecture and protomer tertiary structure suggest parallels in the underlying contraction mechanism for all systems. In the T4 phage, contraction is generally described as a wave-like process, which is initiated in the baseplate and perpetuates along the helical axis to the apical ends (Figure 5) [119,126]. The contraction movement pushes the needle towards the cell membrane and additionally confers a rotational movement of approx. 360° to it [19]. So in fact, the needle is drilled into the target cell.
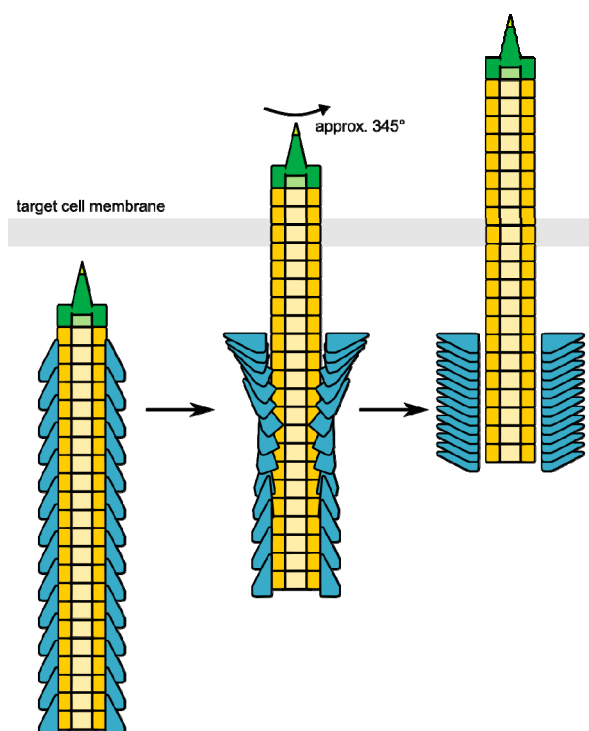

Figure 5. Wave-like contraction process of phage tail-like structures. *Left:* The elongated sheath is in contact with the needle complex. *Middle:* A contraction signal is transferred via the base plate or putatively the membrane complex to the first layer of the tail sheath. The individual protomers tilt and move radially outwards, thereby widening the inner diameter to liberate the needle. Layers closely interdigitate, which leads to shortening of the sheath structure. Rings more distant from the baseplate/membrane complex are still in contact with the needle and rotate and push the needle outwards. *Right:* The fully contracted sheath is shortened to less than half of its original length.

This process was modeled first based on fits of the gp18M crystal structure into the EM reconstructions of the elongated and contracted T4 phage tail (Figure 6), but has been shown to be valid also in the light of the recent reconstructions of the R2 pyocin [11,114]. The contraction process is explained by rigid body movements of the asymmetric unit, with the "swapped", terminal β strand extensions acting as hinges. Although in the original model all gp18 domains were described, domain III and IV, which are conserved in all contractile structures, are sufficient to describe the contraction
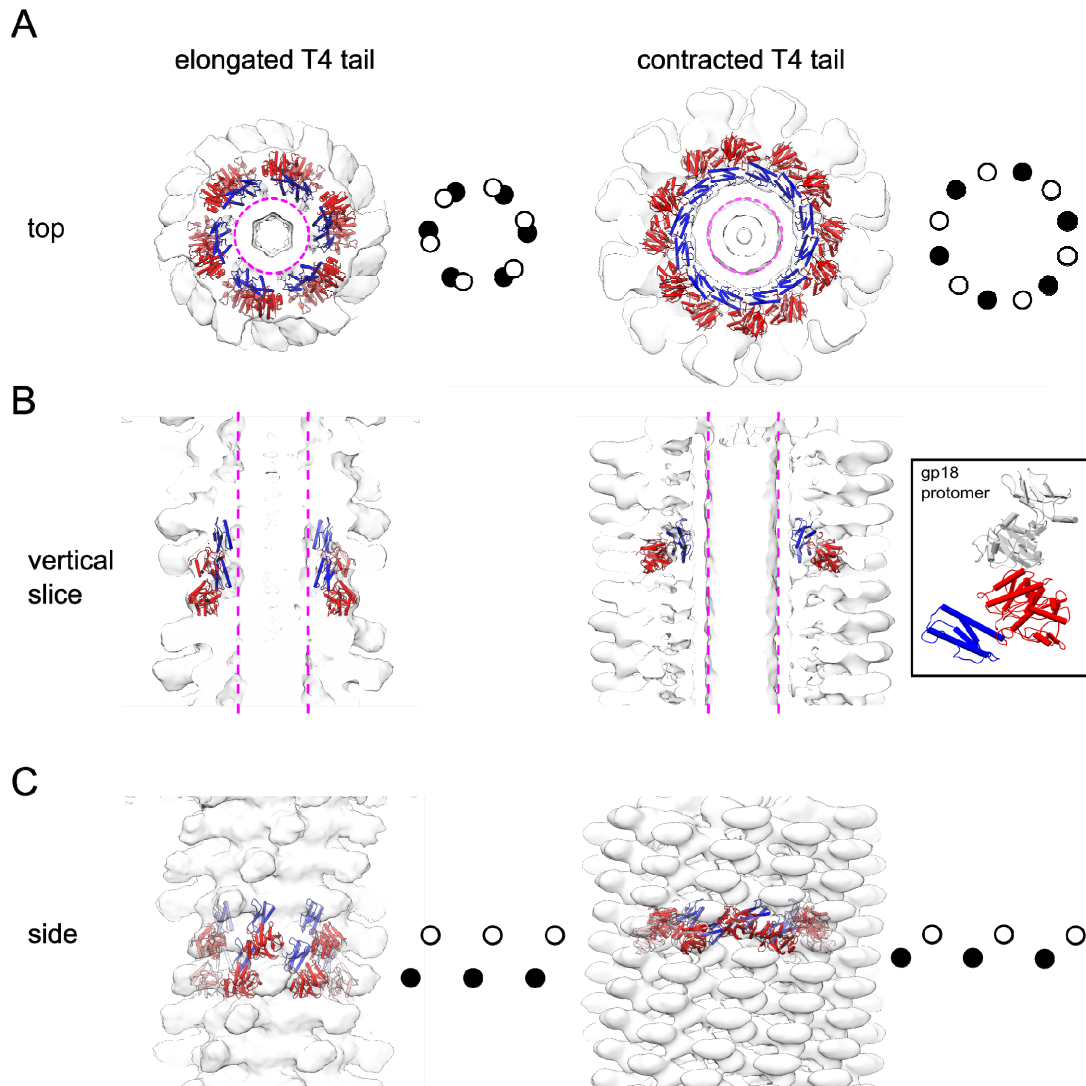
movement (Figure 7 A).

Figure 6. Assembly and contraction mechanism of the T4 sheath. Two consecutive annuli of gp18 hexamers in the conformation of the elongated (pdb-id: 3J2M) or the contracted (pdb-id: 3J2N) T4 phage tail are overlaid with the EM densities (white) of the elongated (EMD-1126) and the contracted (EMD-1086) T4 phage tail and shown as a top view (A), as a central vertical slice through the density (B) and as a side view (C). Only domains gp18 III and IV are shown and colored as in the inset: conserved domain III (red), IV (blue) and PRFI/II domains (white) of gp18 (pdb-id 3J2M). Density attributed to the needle complex is outlined (magenta) and the relative positions of the asymmetric units in the two consecutive rings schematically presented as white and black circle (A and C).
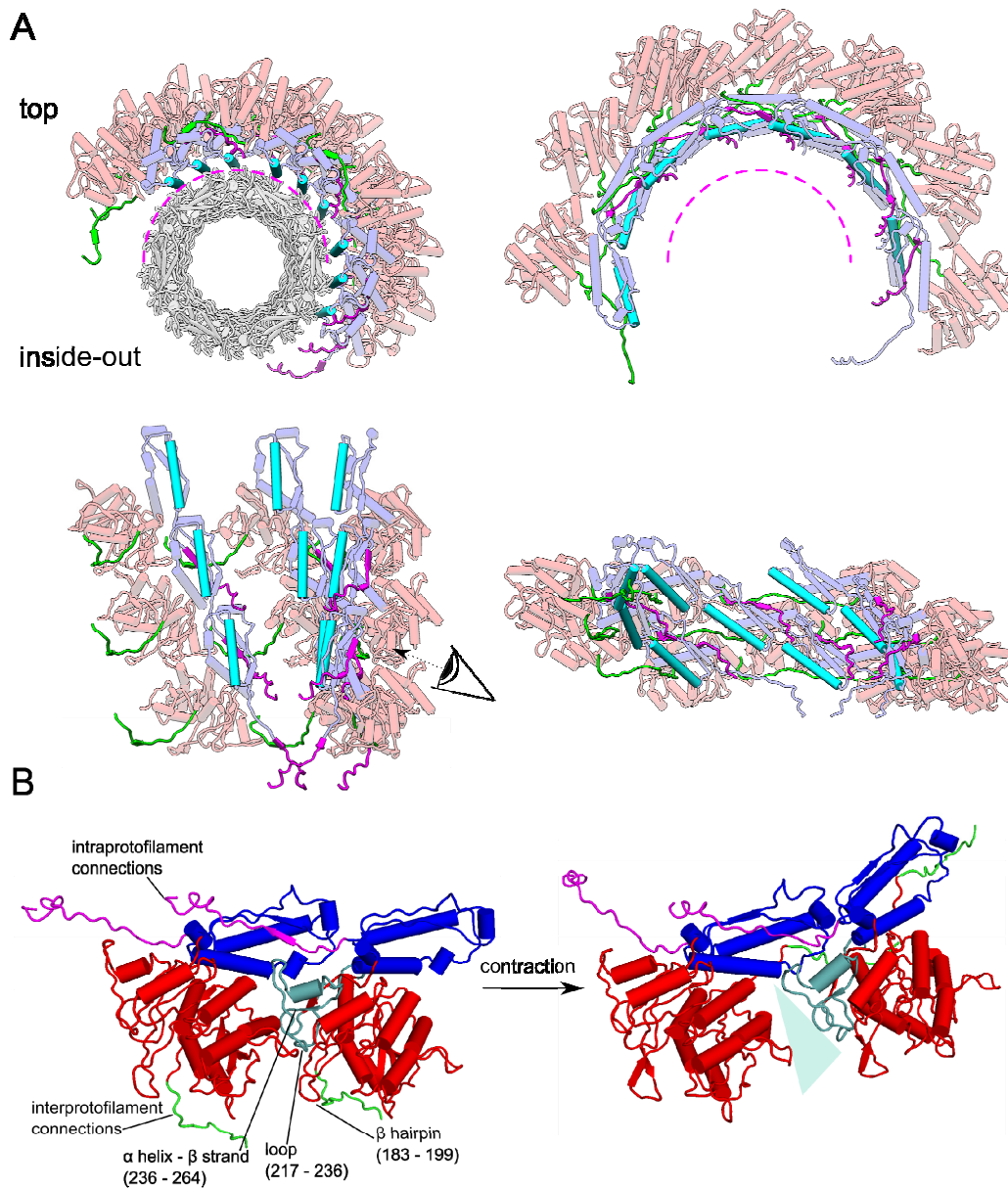
Figure 7. Structural elements in the tail sheath protein involved in polymerization and contraction. (A) Three consecutive R2 tail sheath proteins of three neighboring protofilaments are presented in the elongated (pdb-id 3J9Q) and the contracted (pdb-id 3J9R) conformation as seen from the top and the inside of the tubule. The tail tube (grey) is shown in the representation of the elongated state. The circumference of the tail tube is indicated (magenta) and the most C-terminal α helix of domain IV marked in cyan. The N-terminal arm of domain III forming inter-protofilament connections to domain IV of neighboring protomers in the ring is shown in green, the C-terminal arm of domain IV forming intra-protofilament connections to domain IV of preceding protomers in magenta. (B) Two protomers of one protofilament are represented in the elongated and contracted state as seen as indicated in A. The loop (217–236) and the succeeding polypeptide stretch that influences polymerization properties (236–264) [118,120] are colored light blue. The

change in the interface between protomers is indicated. Domains III and IV are colored as in Figure 6.

As mentioned above, the contraction is initiated by a conformational change of the baseplate (or membrane complex) to the first annulus of the elongated sheath. In R2 pyocins, protomers glide in a rigid body movement ~25 Å radially outwards and ~15° around the axis while rotating 85°, around an axis orthogonal to the helix axis [11]. Contacts between protofilaments in one annulus are broken up, while intra-protofilament contacts maintained by domain IV persist [114]. A C-terminal α helix in domain IV, which is involved in stabilization of the elongated state [11,121] is accessible at the inner tubule wall and is part of the interface between sheath and tail tube (marked in cyan, Figure 7 A). The interaction between sheath and tube is released when the sheath protomers move outwards. As the movement is transmitted to the consecutive annulus, the protomers of the following ring are inserted into the newly formed gaps of the first ring, which reduces the height of the sheath by more than half. New contacts are formed between domain III of neighboring protomers, increasing the contact area by 1,145 $Å^2$ in R2 pyocin structures [5,11]. The increased inter-subunit binding energy accounts for the enthalpy gain during contraction [11,114]. Recent high-resolution structures of the T6SS and R2 pyocin reveal a strong connectivity between individual protomers via β strand swapping. The sheath thus resembles a mesh that ensures contraction signal relaying from the baseplate along the tubule and maintains structural integrity of the sheath during contraction. A strand exchange mechanism between neighbouring protomers most likely drives the directed contraction. Strand exchange has also been suggested to fasten the tubule to the membrane complex via gp25/TssE [15].

Interestingly, spectroscopic analysis of elongated and contracted T4 phage tails and R-Type pyocins suggests that contraction process might be accompanied by a change in the secondary structure content, with a decrease in α helical and an increase in β sheet content [127,128]. Loop 484/510 at the C-terminus of domain III precedes the α/β motif, necessary for tubule polymerization [114,118,120]. This loop was found to influence the position of a nearby β hairpin (aa 454–470) in the gp18M structure [114]. Loop and hairpin are located at the interface between protomers of the same protofilament (Figure 7 B). This contact area changes during contraction as protomers rotate and slide against each other when the curvature of the protofilaments is increased [114]. However, comparing pyocin protomer structures of the elongated and contracted tubules, the secondary structure elements in this region remain unchanged.

6. Conclusions

Phage tail-like machineries are composed of a conserved set of building parts forming the needle, a contractile sheath and a protein platform onto which the system is assembled. Even though all systems share a conserved core, the individual parts are adapted to a variety of functions. Yet, early investigation of the bacteriophage T4 system resulted in a model of action for the contractile machinery, which seems valid for the whole family of different machineries. Molecular details concerning the initiation of contraction and the interaction between sheath and needle remain to be revealed. Investigation of related systems can contribute to the field and help to distinguish common and specialized features of each system.

Cryo EM reconstructions have proven to be essential for the progress in the field as they allow

direct visualization of the interplay of proteins in huge multimeric complexes in different conformational states. The resolution that can be reached by cryo EM methods today has improved due to new detectors and methods of data processing [129], which will facilitate further investigation of these systems at a pseudo-atomic level.

Acknowledgments

Conflict of Interest

The authors declare no conflict of interest.

References

1. Leiman PG, Shneider MM (2012) Contractile tail machines of bacteriophages. In: Rossmann MG, Rao VB, editors. *Viral Molecular Machines*. New York Dordrecht Heidelberg London: Springer. 93–114.
2. Michel-Briand Y, Baysse C (2002) The pyocins of Pseudomonas aeruginosa. *Biochimie* 84: 499–510.
3. Sarris PF, Ladoukakis ED, Panopoulos NJ, et al. (2014) A phage tail-derived element with wide distribution among both prokaryotic domains: a comparative genomic and phylogenetic study. *Genome Biol Evol* 6: 1739–1747.
4. Amos LA, Klug A (1975) Three-dimensional image reconstructions of the contractile tail of T4 bacteriophage. *J Mol Biol* 99: 51–64.
5. Leiman PG, Chipman PR, Kostyuchenko VA, et al. (2004) Three-dimensional rearrangement of proteins in the tail of bacteriophage T4 on infection of its host. *Cell* 118: 419–429.
6. Kostyuchenko VA, Chipman PR, Leiman PG, et al. (2005) The tail structure of bacteriophage T4 and its mechanism of contraction. *Nat Struct Mol Biol* 12: 810–813.
7. Effantin G, Hamasaki R, Kawasaki T, et al. (2013) Cryo-electron microscopy three-dimensional structure of the jumbo phage PhiRSL1 infecting the phytopathogen Ralstonia solanacearum. *Structure* 21: 298–305.
8. Fokine A, Battisti AJ, Bowman VD, et al. (2007) Cryo-EM study of the Pseudomonas bacteriophage phiKZ. *Structure* 15: 1099–1104.
9. Aksyuk AA, Kurochkina LP, Fokine A, et al. (2011) Structural conservation of the myoviridae phage tail sheath protein fold. *Structure* 19: 1885–1894.
10. Schwarzer D, Buettner FF, Browning C, et al. (2012) A multivalent adsorption apparatus explains the broad host range of phage phi92: a comprehensive genomic and structural analysis. *J Virol* 86: 10384–10398.
11. Ge P, Scholl D, Leiman PG, et al. (2015) Atomic structures of a bactericidal contractile nanotube in its pre- and postcontraction states. *Nat Struct Mol Biol*.

12. Basler M, Pilhofer M, Henderson GP, et al. (2012) Type VI secretion requires a dynamic contractile phage tail-like structure. *Nature* 483: 182–186.

13. Kube S, Kapitein N, Zimniak T, et al. (2014) Structure of the VipA/B type VI secretion complex suggests a contraction-state-specific recycling mechanism. *Cell Rep* 8: 20–30.

14. Clemens DL, Ge P, Lee BY, et al. (2015) Atomic structure of T6SS reveals interlaced array essential to function. *Cell* 160: 940–951.

15. Kudryashev M, Wang RY, Brackmann M, et al. (2015) Structure of the type VI secretion system contractile sheath. *Cell* 160: 952–962.

16. Heymann JB, Bartho JD, Rybakova D, et al. (2013) Three-dimensional structure of the toxin-delivery particle antifeeding prophage of Serratia entomophila. *J Biol Chem* 288: 25276–25284.

17. Shikuma NJ, Pilhofer M, Weiss GL, et al. (2014) Marine tubeworm metamorphosis induced by arrays of bacterial phage tail-like structures. *Science* 343: 529–533.

18. Veesler D, Cambillau C (2011) A common evolutionary origin for tailed-bacteriophage functional modules and bacterial machineries. *Microbiol Mol Biol Rev* 75: 423–433.

19. Leiman PG, Arisaka F, van Raaij MJ, et al. (2010) Morphogenesis of the T4 tail and tail fibers. *Virology* 7: 355.

20. Silverman JM, Brunet YR, Cascales E, et al. (2012) Structure and regulation of the type VI secretion system. *Annu Rev Microbiol* 66: 453–472.

21. Ho BT, Dong TG, Mekalanos JJ (2014) A view to a kill: the bacterial type VI secretion system. *Cell Host Microbe* 15: 9–21.

22. Zoued A, Brunet YR, Durand E, et al. (2014) Architecture and assembly of the Type VI secretion system. *Biochim Biophys Acta Mol Cell Res* 1843: 1664–1673.

23. Nakayama K, Takashima K, Ishihara H, et al. (2000) The R-type pyocin of Pseudomonas aeruginosa is related to P2 phage, and the F-type is related to lambda phage. *Mol Microbiol* 38: 213–231.

24. Liu Y, Schmidt B, Maskell DL (2010) MSAProbs: multiple sequence alignment based on pair hidden Markov models and partition function posterior probabilities. *Bioinformatics* 26: 1958–1964.

25. Felsenstein J (1989) Phylip: phylogeny inference package (version 3.2). *Cladistics* 5: 164–166.

26. Ackermann HW (2006) Classification of bacteriophages. In: Calendar R, editor. *The Bacteriophages*. New York, USA: Oxford University Press. 8–16.

27. Orlova EV (2012) Bacteriophages and their structural organisation. *Bacteriophages* 3–30.

28. Ruska H (1942) Morphologische Befunde bei der bakteriophagen Lyse. *Arch Gesamte Virusforsch* 2: 345–387.

29. Ackermann HW (2011) The first phage electron micrographs. *Bacteriophage* 1: 225–227.

30. De Rosier DJ, Klug A (1968) Reconstruction of three dimensional structures from electron micrographs. *Nature* 217: 130–134.

31. Jacob F (1954) Induced biosynthesis and mode of action of a pyocine, antibiotic produced by Pseudomonas aeruginosa. *Annales de l'Institut Pasteur* 86: 149–160.

32. Takeya K, Mlnamishima Y, Amako K, et al. (1967) A small rod-shaped pyocin. *Virology* 31: 166–168.

33. Ishii SI, Nishi Y, Egami F (1965) The fine structure of a pyocin. *J Mol Biol* 13: 428–431.

34. Shinomiya T, Shiga S, Kageyama M (1983) Genetic determinant of pyocin R2 in Pseudomonas

aeruginosa PAO. I. Localization of the pyocin R2 gene cluster between the trpCD and trpE genes. *Mol Gen Genet* 189: 375–381.

35. Birmingham VA, Pattee PA (1981) Genetic transformation in Staphylococcus aureus: isolation and characterization of a competence-conferring factor from bacteriophage 80 alpha lysates. *J Bacteriol* 148: 301–307.

36. Coetzee HL, de Klerk HC, Coetzee JN, et al. (1968) Bacteriophage-tail-like Particles Associated with Intra-species Killing of Proteus vulgaris. *J Gen Virol* 2: 29–36.

37. Gebhart D, Williams SR, Bishop-Lilly KA, et al. (2012) Novel high-molecular-weight, R-type bacteriocins of Clostridium difficile. *J Bacteriol* 194: 6240–6247.

38. Matsui H, Sano Y, Ishihara H, et al. (1993) Regulation of pyocin genes in Pseudomonas aeruginosa by positive (prtN) and negative (prtR) regulatory genes. *J Bacteriol* 175: 1257–1263.

39. Scholl D, Cooley M, Williams SR, et al. (2009) An engineered R-type pyocin is a highly specific and sensitive bactericidal agent for the food-borne pathogen Escherichia coli O157:H7. *Antimicrob Agents Chemother* 53: 3074–3080.

40. Williams SR, Gebhart D, Martin DW, et al. (2008) Retargeting R-type pyocins to generate novel bactericidal protein complexes. *Appl Environ Microbiol* 74: 3868–3876.

41. Uratani Y, Hoshino T (1984) Pyocin R1 inhibits active transport inPseudomonas aeruginosa and depolarizes membrane potential. *J Bacteriol* 157: 632–636.

42. Strauch E, Kaspar H, Schaudinn C, et al. (2001) Characterization of Enterocoliticin, a Phage Tail-Like Bacteriocin, and Its Effect on Pathogenic Yersinia enterocolitica Strains. *Appl Environ Microbiol* 67: 5634–5642.

43. Ito S, Kageyama M, Egami F (1970) Isolation and characterization of pyocins from several strains of Pseudomonas aeruginosa. *J Gen Appl Microbiol* 16: 205–214.

44. Rodou A, Ankrah DO, Stathopoulos C (2010) Toxins and secretion systems of Photorhabdus luminescens. *Toxins* 2: 1250–1264.

45. Yang G, Dowling AJ, Gerike U, et al. (2006) Photorhabdus virulence cassettes confer injectable insecticidal activity against the wax moth. *J Bacteriol* 188: 2254–2261.

46. Hurst MRH, Beard SS, Jackson TA, et al. (2007) Isolation and characterization of the Serratia entomophila antifeeding prophage. *FEMS Microbiol Lett* 270: 42–48.

47. Rybakova D, Radjainia M, Turner A, et al. (2013) Role of antifeeding prophage (Afp) protein Afp16 in terminating the length of the Afp tailocin and stabilizing its sheath. *Mol Microbiol* 89: 702–714.

48. Rybakova D, Schramm P, Mitra AK, et al. (2015) Afp14 is involved in regulating the length of Anti-feeding prophage (Afp). *Mol Microbiol*.

49. Ogata S, Suenaga H, Hayashida S (1982) Pock Formation of Streptomycetes endus with Production of Phage Taillike Particles. *Appl Environ Microbiol* 43: 1182–1187.

50. Mougous JD, Cuff ME, Raunser S, et al. (2006) A virulence locus of Pseudomonas aeruginosa encodes a protein secretion apparatus. *Science* 312: 1526–1530.

51. Pukatzki S, Ma AT, Sturtevant D, et al. (2006) Identification of a conserved bacterial protein secretion system in Vibrio cholerae using the Dictyostelium host model system. *Proc Natl Acad Sci USA* 103: 1528–1533.

52. Bingle LE, Bailey CM, Pallen MJ (2008) Type VI secretion: a beginner's guide. *Curr Opin Microbiol* 11: 3–8.

53. Boyer F, Fichant G, Berthod J, et al. (2009) Dissecting the bacterial type VI secretion system by

a genome wide in silico analysis: what can be learned from available microbial genomic resources? *BMC Genomics* 10: 104.

54. Bröms JE, Sjöstedt A, Lavander M (2010) The Role of the Francisella tularensis Pathogenicity Island in Type VI Secretion, Intracellular Survival, and Modulation of Host Cell Signaling. *Front Microbiol* 1: 136–136.

55. de Bruin OM, Duplantis BN, Ludu JS, et al. (2011) The biochemical properties of the Francisella Pathogenicity Island (FPI)-encoded proteins, IglA, IglB, IglC, PdpB and DotU, suggest roles in type VI secretion. *Microbiology*.

56. Russell AB, Wexler AG, Harding BN, et al. (2014) A type VI secretion-related pathway in Bacteroidetes mediates interbacterial antagonism. *Cell Host Microbe* 16: 227–236.

57. Shalom G, Shaw JG, Thomas MS (2007) In vivo expression technology identifies a type VI secretion system locus in Burkholderia pseudomallei that is induced upon invasion of macrophages. *Microbiology* 153: 2689–2699.

58. Leiman PG, Basler M, Ramagopal UA, et al. (2009) Type VI secretion apparatus and phage tail-associated protein complexes share a common evolutionary origin. *Proc Natl Acad Sci USA* 106: 4154–4159.

59. Pell LG, Kanelis V, Donaldson LW, et al. (2009) The phage lambda major tail protein structure reveals a common evolution for long-tailed phages and the type VI bacterial secretion system. *Proc Natl Acad Sci USA* 106: 4160–4165.

60. Lossi NS, Dajani R, Freemont P, et al. (2011) Structure-function analysis of HsiF, a gp25-like component of the type VI secretion system, in Pseudomonas aeruginosa. *Microbiology* 157: 3292–3305.

61. Bonemann G, Pietrosiuk A, Diemand A, et al. (2009) Remodelling of VipA/VipB tubules by ClpV-mediated threading is crucial for type VI protein secretion. *EMBO J* 28: 315–325.

62. Lossi NS, Manoli E, Forster A, et al. (2013) The HsiB1C1 (TssB-TssC) complex of the Pseudomonas aeruginosa type VI secretion system forms a bacteriophage tail sheathlike structure. *J Biol Chem* 288: 7536–7548.

63. Zheng J, Ho B, Mekalanos JJ (2011) Genetic analysis of anti-amoebae and anti-bacterial activities of the type VI secretion system in Vibrio cholerae. *PLoS One* 6: e23876–e23876.

64. Zoued A, Durand E, Bebeacua C, et al. (2013) TssK is a trimeric cytoplasmic protein interacting with components of both phage-like and membrane anchoring complexes of the type VI secretion system. *J Biol Chem* 288: 27031–27041.

65. Durand E, Zoued A, Spinelli S, et al. (2012) Structural characterization and oligomerization of the TssL protein, a component shared by bacterial type VI and type IVb secretion systems. *J Biol Chem* 287: 14157–14168.

66. Robb CS, Nano FE, Boraston AB (2012) The structure of the conserved type six secretion protein TssL (DotU) from Francisella novicida. *J Mol Biol* 419: 277–283.

67. Ma LS, Lin JS, Lai EM (2009) An IcmF family protein, ImpLM, is an integral inner membrane protein interacting with ImpKL, and its walker a motif is required for type VI secretion system-mediated Hcp secretion in Agrobacterium tumefaciens. *J Bacteriol* 191: 4316–4329.

68. Das S, Chaudhuri K (2003) Identification of a unique IAHP (IcmF associated homologous proteins) cluster in Vibrio cholerae and other proteobacteria through in silico analysis. *In Silico Biol* 3: 287–300.

69. Felisberto-Rodrigues C, Durand E, Aschtgen MS, et al. (2011) Towards a Structural

Comprehension of Bacterial Type VI Secretion Systems: Characterization of the TssJ-TssM Complex of an Escherichia coli Pathovar. *PLoS Pathog* 7: e1002386.

70. Rao VA, Shepherd SM, English G, et al. (2011) The structure of Serratia marcescens Lip, a membrane-bound component of the type VI secretion system. *Acta Crystallogr D Biol Crystallogr* 67: 1065–1072.

71. Miyata ST, Bachmann V, Pukatzki S (2013) Type VI secretion system regulation as a consequence of evolutionary pressure. *J Med Microbiol* 62: 663–676.

72. Bernard CS, Brunet YR, Gavioli M, et al. (2011) Regulation of type VI secretion gene clusters by sigma54 and cognate enhancer binding proteins and cognate enhancer binding proteins. *Journal of bacteriology* 193: 2158–2167.

73. Kitaoka M, Miyata ST, Brooks TM, et al. (2011) VasH is a transcriptional regulator of the type VI secretion system functional in endemic and pandemicVibrio cholerae. *J Bacteriology* 193: 6471–6482.

74. Dong TG, Mekalanos JJ (2012) Characterization of the RpoN regulon reveals differential regulation of T6SS and new flagellar operons in Vibrio cholerae O37 strain V52. *Nucleic acids research* 40: 7766–7775.

75. Basler M, Ho BT, Mekalanos JJ (2013) Tit-for-tat: type VI secretion system counterattack during bacterial cell-cell interactions. *Cell* 152: 884–894.

76. Basler M, Mekalanos JJ (2012) Type 6 secretion dynamics within and between bacterial cells. *Science* 337: 815.

77. Ho BT, Basler M, Mekalanos JJ (2013) Type 6 secretion system-mediated immunity to type 4 secretion system-mediated gene transfer. *Science* 342: 250–253.

78. Fritsch MJ, Trunk K, Diniz JA, et al. (2013) Proteomic Identification of Novel Secreted Antibacterial Toxins of the Serratia marcescens Type VI Secretion System. *Mol Cell Proteomics* 12: 2735–2749.

79. Mougous JD, Gifford CA, Ramsdell TL, et al. (2007) Threonine phosphorylation post-translationally regulates protein secretion in Pseudomonas aeruginosa. *Nat Cell Biol* 9: 797–803.

80. Kapitein N, Bonemann G, Pietrosiuk A, et al. (2013) ClpV recycles VipA/VipB tubules and prevents non-productive tubule formation to ensure efficient type VI protein secretion. *Mol Microbiol* 87: 1013–1028.

81. Hsu F, Schwarz S, Mougous JD (2009) TagR promotes PpkA-catalysed type VI secretion activation in Pseudomonas aeruginosa. *Mol Microbiol* 72: 1111–1125.

82. Silverman JM, Austin LS, Hsu F, et al. (2011) Separate inputs modulate phosphorylation-dependent and -independent type VI secretion activation. *Mol Microbiol* 82: 1277–1290.

83. Casabona MG, Silverman JM, Sall KM, et al. (2013) An ABC transporter and an outer membrane lipoprotein participate in posttranslational activation of type VI secretion in Pseudomonas aeruginosa. *Environ Microbiol* 15: 471–486.

84. Lin JS, Wu HH, Hsu PH, et al. (2014) Fha interaction with phosphothreonine of TssL activates type VI secretion in Agrobacterium tumefaciens. *PLoS Pathog* 10: e1003991–e1003991.

85. Zheng J, Leung KY (2007) Dissection of a type VI secretion system in Edwardsiella tarda. *Mol Microbiol* 66: 1192–1206.

86. Ma LS, Narberhaus F, Lai EM (2012) IcmF family protein TssM exhibits ATPase activity and

energizes type VI secretion. *J Biol Chem* 287: 15610–15621.

87. Shneider MM, Buth SA, Ho BT, et al. (2013) PAAR-repeat proteins sharpen and diversify the type VI secretion system spike. *Nature* 500: 350–353.

88. Brunet YR, Hénin J, Celia H, et al. (2014) Type VI secretion and bacteriophage tail tubes share a common assembly pathway. *EMBO Rep* 15: 315–321.

89. Bröms JE, Lavander M, Sjöstedt A (2009) A conserved alpha-helix essential for a type VI secretion-like system of Francisella tularensis. *J Bacteriol* 191: 2431–2446.

90. Aubert DF, MacDonald DK, Valvano MA (2010) BcsKC is an essential protein for the type VI secretion system activity in Burkholderia cenocepacia that forms an outer membrane complex with BcsLB. *J Biol Chem* 285: 35988–35998.

91. Chang YW, Chen S, Tocheva EI, et al. (2014) Correlated cryogenic photoactivated localization microscopy and cryo-electron tomography. *Nature Methods* 11: 737–739.

92. King J (1971) Bacteriophage T4 tail assembly: four steps in core formation. *J Mol Biol* 58: 693–709.

93. Silverman JM, Agnello DM, Zheng H, et al. (2013) Haemolysin coregulated protein is an exported receptor and chaperone of type VI secretion substrates. *Mol Cell* 51: 584–593.

94. Brooks TM, Unterweger D, Bachmann V, et al. (2013) Lytic activity of the Vibrio cholerae type VI secretion toxin VgrG-3 is inhibited by the antitoxin TsaB. *J Biol Chem* 288: 7618–7625.

95. Pietrosiuk A, Lenherr ED, Falk S, et al. (2011) Molecular basis for the unique role of the AAA+ chaperone ClpV in type VI protein secretion. *J Biol Chem* 286: 30010–30021.

96. Forster A, Planamente S, Manoli E, et al. (2014) Coevolution of the ATPase ClpV, the Sheath Proteins TssB and TssC and the Accessory Protein TagJ/HsiE1 Distinguishes Type VI Secretion Classes. *J Biol Chem* 289: 33032–33043.

97. King J (1968) Assembly of the tail of bacteriophage T4. *J Mol Biol* 32: 231–262.

98. Abuladze NK, Gingery M, Tsai J, et al. (1994) Tail length determination in bacteriophage T4. *Virology* 199: 301–310.

99. Kanamaru S, Leiman PG, Kostyuchenko VA, et al. (2002) Structure of the cell-puncturing device of bacteriophage T4. *Nature* 415: 553–557.

100. Kanamaru S, Ishiwata Y, Suzuki T, et al. (2005) Control of bacteriophage T4 tail lysozyme activity during the infection process. *J Mol Biol* 346: 1013–1020.

101. Pukatzki S, Ma AT, Revel AT, et al. (2007) Type VI secretion system translocates a phage tail spike-like protein into target cells where it cross-links actin. *Proc Natl Acad Sci USA* 104: 15508–15513.

102. Ma AT, McAuley S, Pukatzki S, et al. (2009) Translocation of a Vibrio cholerae type VI secretion effector requires bacterial endocytosis by host cells. *Cell Host Microbe* 5: 234–243.

103. Suarez G, Sierra JC, Erova TE, et al. (2010) A type VI secretion system effector protein, VgrG1, from Aeromonas hydrophila that induces host cell toxicity by ADP ribosylation of actin. *J Bacteriol* 192: 155–168.

104. Durand E, Derrez E, Audoly G, et al. (2012) Crystal structure of the VgrG1 actin cross-linking domain of the Vibrio cholerae type VI secretion system. *J Biol Chem* 287: 38190–38199.

105. Browning C, Shneider MM, Bowman VD, et al. (2012) Phage pierces the host cell membrane with the iron-loaded spike. *Structure* 20: 326–339.

106. Moody MF, Makowski L (1981) X-ray diffraction study of tail-tubes from bacteriophage T2L. *J Mol Biol* 150: 217–244.

107. Wagenknecht T, Bloomfield VA (1977) In vitro polymerization of bacteriophage T4D tail core subunits. *J Mol Biol* 116: 347–359.

108. Poglazov BF, Nikolskaya TI (1969) Self-assembly of the protein of bacteriophage T2 tail cores. *J Mol Biol* 43: 231–233.

109. Douzi B, Spinelli S, Blangy S, et al. (2014) Crystal structure and self-interaction of the type VI secretion tail-tube protein from enteroaggregative Escherichia coli. *PLoS One* 9: e86918–e86918.

110. Lin JS, Ma LS, Lai EM (2013) Systematic dissection of the agrobacterium type VI secretion system reveals machinery and secreted components for subcomplex formation. *PLoS One* 8: e67647–e67647.

111. Kostyuchenko VA, Leiman PG, Chipman PR, et al. (2003) Three-dimensional structure of bacteriophage T4 baseplate. *Nat Struct Mol Biol* 10: 688–693.

112. Lim YT, Jobichen C, Wong J, et al. (2015) Extended loop region of Hcp1 is critical for the assembly and function of type VI secretion system in Burkholderia pseudomallei. *Sci Rep* 5: 8235.

113. Jobichen C, Chakraborty S, Li M, et al. (2010) Structural basis for the secretion of EvpC: a key type VI secretion system protein from Edwardsiella tarda. *PLoS One* 5: e12910.

114. Aksyuk AA, Leiman PG, Kurochkina LP, et al. (2009) The tail sheath structure of bacteriophage T4: a molecular machine for infecting bacteria. *EMBO J* 28: 821–829.

115. Fokine A, Zhang Z, Kanamaru S, et al. (2013) The molecular architecture of the bacteriophage T4 neck. *J Mol Biol* 425: 1731–1744.

116. Broms JE, Ishikawa T, Wai SN, et al. (2013) A functional VipA-VipB interaction is required for the type VI secretion system activity of Vibrio cholerae O1 strain A1552. *BMC Microbiol* 13: 96.

117. Zhang XY, Brunet YR, Logger L, et al. (2013) Dissection of the TssB-TssC Interface during Type VI Secretion Sheath Complex Formation. *PLoS One* 8: e81074.

118. Poglazov BF, Efimov AV, Marco S, et al. (1999) Polymerization of bacteriophage T4 tail sheath protein mutants truncated at the C-termini. *J Struct Biol* 127: 224–230.

119. Moody MF (1973) Sheath of bacteriophage T4. 3. Contraction mechanism deduced from partially contracted sheaths. *J Mol Biol* 80: 613–635.

120. Efimov AV, Kurochkina LP, Mesyanzhinov VV (2002) Engineering of bacteriophage T4 tail sheath protein. *Biochemistry (Moscow)* 67: 1366–1370.

121. Takeda S, Suzuki M, Yamada T, et al. (2004) Mapping of functional sites on the primary structure of the contractile tail sheath protein of bacteriophage T4 by mutation analysis. *Biochim Biophys Acta, Proteins Proteom* 1699: 163–171.

122. Maxwell KL, Fatehi HM, Chang T, et al. (2013) Structural and functional studies of gpX of Escherichia coli phage P2 reveal a widespread role for LysM domains in the baseplates of contractile-tailed phages. *J Bacteriol* 195: 5461–5468.

123. Bradley DE (1963) The structure of coliphages. *J Gen Microbiol* 31: 435–445.

124. Leblanc C, Caumont-Sarcos A, Comeau AM, et al. (2009) Isolation and genomic characterization of the first phage infecting Iodobacteria: varphiPLPE, a myovirus having a novel set of features. *Env Microbiol Rep* 1: 499–509.

125. Moody MF (1967) Structure of the sheath of bacteriophage T4. I. Structure of the contracted sheath and polysheath. *J Mol Biol* 25: 167–200.

126. Moody MF (1967) Structure of the sheath of bacteriophage T4. II. Rearrangement of the sheath subunits during contraction. *J Mol Biol* 25: 201–208.
127. Uratani Y (1982) A circular dichroism study of sheath contraction in pyocin R1. *Biochim Biophys Acta* 703: 196–203.
128. Venyaminov SY, Rodikova LP, Metlina AL, et al. (1975) Secondary structure change of bacteriophage T4 sheath protein during sheath contraction. *J Mol Biol* 98: 657–664.
129. Bai X-c, McMullan G, Scheres SHW (2015) How cryo-EM is revolutionizing structural biology. *Trends Biochem Sci* 40: 49–57.
130. Pettersen EF, Goddard TD, Huang CC, et al. (2004) UCSF Chimera--a visualization system for exploratory research and analysis. *J Comput Chem* 25: 1605–1612.